J. R. Castrejon-Pita, S. D. Hoath, A. A. Castrejon-Pita, N. F. Morrison, W.-K. Hsiao and I. M. Hutchings, in Proc 27th Int. Conf. on Digital Printing Technologies, NIP27, Minneapolis, MN, USA, 2011, 93-96, 'Ultra-High Speed Particle Image Velocimetry on Drop-on-Demand Jetting'

Ultra-High Speed Particle Image Velocimetry on Drop-on-Demand Jetting

SCHOLARONE™
Manuscripts

Ultra-High Speed Particle Image Velocimetry on Drop-on-Demand Jetting

José R. Castrejón-Pita, Stephen D. Hoath, Alfonso A. Castrejón-Pita, Neil F. Morrison[*], Wen-Kai Hsiao and Ian M. Hutchings
Inkjet Research Centre, University of Cambridge, 17 Charles Babbage Road, Cambridge CB3 0FS, UK
[*]*Department of Applied Mathematics, University of Leeds, Leeds, LS2 9JT, UK.*

Abstract

An experimental setup to study the dynamics of droplet jetting from a commercially available print-head is described. A MicroFab print-head with an 80 µm diameter transparent nozzle was set to print droplets at a speed of 5 m/s at a frequency of 7 kHz. A Particle Image Velocimetry (PIV) scheme consisting of an optical microscope coupled to an ultra-high speed camera is utilized to capture the motion of particles suspended in a model transparent ink. This experimental arrangement images the flow at the centre of a glass cylindrical nozzle and above the fluid meniscus at a speed of half a million frames per second. Velocity fields are obtained from an approximately 200 µm thickness layer of fluid at the inside of the nozzle. Experimental results are compared with Lagrangian finite-element numerical simulations under identical fluid and jetting conditions with good agreement. The advantages, challenges and current limitations of this approach are discussed.

Introduction

The process of droplet jetting is fundamental to the quality and speed of drop on demand systems. The mechanisms controlling the jetting are varied and range from acoustical effects to pure mechanical forces. In general, these effects can usually be controlled by the properties of the signal driving the actuator that produces the jetting (usually called waveform) [1]. Although several studies have analyzed the effect of waveform characteristics on the drop formation, the conversion of the driving signal to a pressure or speed variation has remained elusive. This is expected as different print-heads are driven by different actuators, have different inner geometries and work with different fluids. In addition to these complications, the sizes and operating speeds of commercially available systems make the measurement of pressures, speeds and nozzle geometries difficult or impossible [2, 3]. Although pressure and speeds have been measured in large scale systems using fluid anemometry techniques, these approaches are not applicable to other systems as they would require optical access to the liquid behind the nozzle [2, 3].

The objective of this work is to present a scheme where the fluid flow within a transparent tapered cylindrical nozzle is visualized by an ultra-high speed camera and its characteristic velocities measured during jetting. These measurements are then feedback to Lagrangian numerical methods for comparison.

Experimental set up

The imaging rig, as shown in Figure 1, consists of a Shimadzu HPV-1 ultra high-speed camera which is capable of capturing 102 full resolution (310 X 260 pixels) gray scale images up to 1,000,000 fps with exposure time down to 0.25 µs. The illumination is provided by an Adapt Electronics Photoflash system which produces 2 ms duration, 500 Joules flashes. Due to the finite warm up time of the light source and consequent strong variation in the illumination, the triggers for the print head firing and camera were slightly delayed (~ 100µs) relative to the trigger to the light source controller (CU-500) using a delayed pulse generator (TTi TGP-110).

A see-through glass nozzle (MicroFab MJ-AB-01-80-6MX) is mounted vertically on a motorized multi-axis positioning stage with its unguarded nozzle directed downwards between the camera and the flash. The camera, fitted with a microscope lens (Navitar 12X ultra zoom with Mitutoyo objectives with long working distance), records shadowgraph images of the fluid lying either within the 80 µm diameter nozzle exit or outside in the jet.
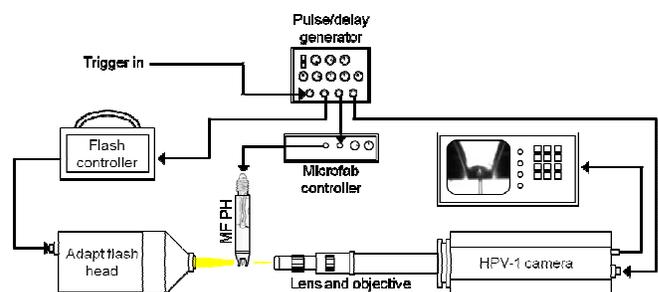

Figure 1. Schematic of the experimental arrangement used in this work.

The model ink used in the present study was a 10cp DEP (diethyl phthalate) fluid seeded with 2.0µm TiO_2 particles. The fluid preparations were as follows: particles were dispersed into a few cc of the warmed solvent, using a magnetic stirrer, and then degassed prior to loading into the jetting rig by using an ultrasonic bath for 15 minutes. The jetting was recorded at 500,000 fps.

Particle Image Velocimetry

Particle Image Velocimetry (PIV) was applied to high speed images to extract velocity maps inside the MicroFab nozzle. In brief, PIV is a technique that works by cross-correlating the intensity distributions over small areas of the flow in a pair of images with a given time separation. By estimating the averaged displacement for each interrogation area, in a known time interval, a velocity vector can be assigned for each of these boxes. Unlike more traditional particle image velocimetry approaches, PIV does not need to resolve the motion of individual tracer particles, and hence is well suited to the analysis of flows with a large degree of spatial scale variation. In the current experiments, the interrogation areas measured 32×32 pixels, and analysed with an overlap of 50% (typical in this kind of flows, [4]), giving an approximate box, in real coordinates, of 13 μm × 13 μm, or a final spatial resolution of roughly 6.5 μm (neglecting optical aberration by the nozzle geometry and refractive indexes). Black and white shadowgraph image pixels need to be inverted prior to application of most PIV analysis packages. Our PIV results are shown superposed in Fig. 2.

In a conventional PIV system, a fluid plane is usually illuminated by a couple of short duration laser pulses. Each of these pulses illuminates the interrogation plane at different times and produces the illumination necessary to capture the averaged position of the seeded particles on the flow. A laser sheet is usually required in such a way that only a thin layer of the fluid, and not a whole volume, is studied. The small lengths size and fast dynamics, together with the high intensity illumination requirements of the ultra-high speed camera used in these experiments, produce a scheme where a continuous laser sheet is practically impossible to generate, given the availability of visible high power lasers and the limitations of most commercially available lenses.

In these experiments, the whole fluid inside the MicroFab nozzle was back illuminated (shadowgraph) by a long duration flash and visualized by a microscope lens which depth of field is comparable to the external diameter of the nozzle (~200 μm). Therefore, in the recorded images, all the particles suspended along the nozzle thickness are approximately in focus. As a result, the measurements obtained by the PIV algorithms correspond to the radially-integrated velocities. By assuming a power-law radial velocity profile, however, it was possible to scale up the maximum velocity at the core of the flow. It can be easily shown that for a uniform density distribution of particles sampled across the nozzle profile, the averaged velocity is a fraction $n/(n+2)$ for an integer n power law of the velocity profile. Assuming this is Poiseuille, $n=2$ and the observed radially averaged value is ½ of the actual central speed. For higher n values, or with a m power law particle density distribution, the radial averaged speed observed lies closer to the n-law central speed by an extra factor of $(m+n+4)/(m+n+2)$. The worst case scaling requirement is to double the PIV measurements.
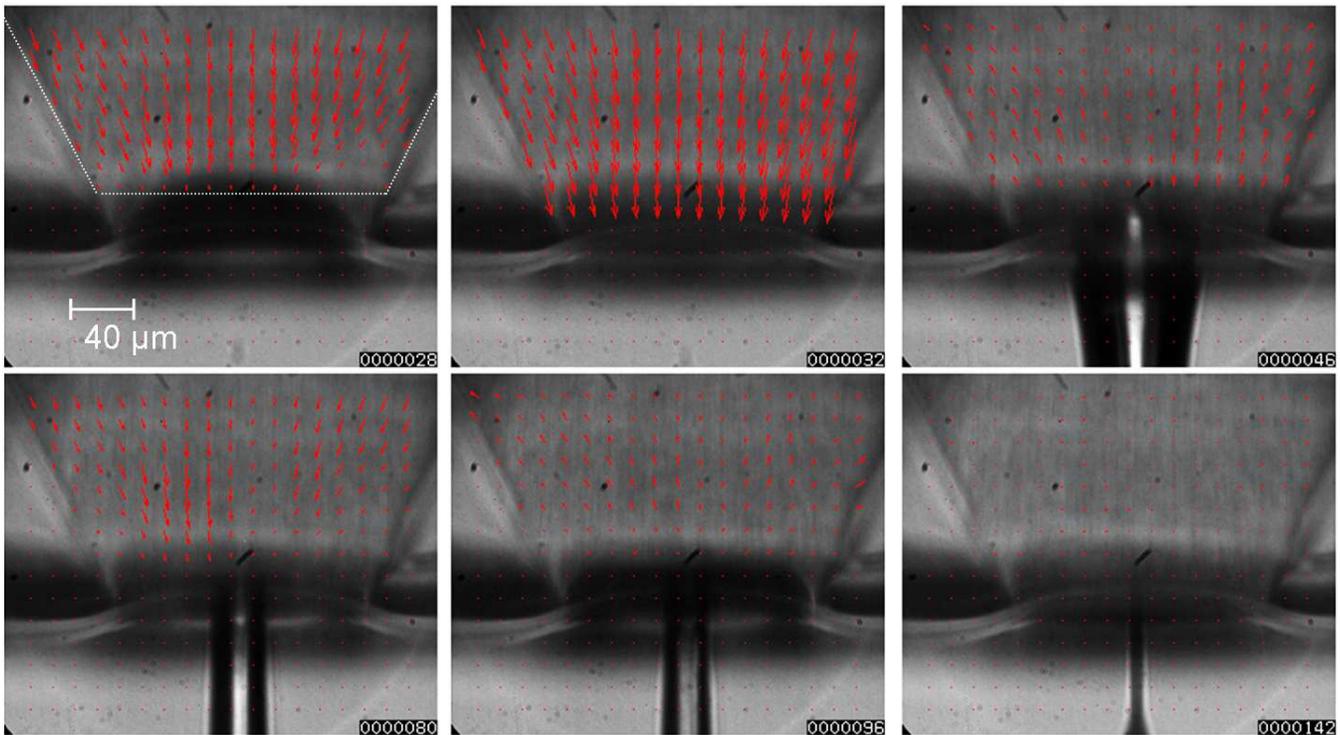

Figure 2. *Images showing the velocity field inside a jetting glass nozzle. The dotted line on the first image shows the mask layout used for the PIV analysis. The fluid, DEP, contains 2 μm TiO$_2$ particles. Images taken by a Shimadzu ultra-high speed camera at a frame rate of 500,000 fps. The image recording time shown in μs (microseconds) at the bottom right corner has 140μs offset from the first drop triggering The scale bar shown outside the glass should be 40 μm. The top right hand picture shows the effects of radial magnification caused by the refractive index of glass: the jetting into air is then approximately at its maximum width = nozzle diameter d =80 μm, but the nozzle appears to be ~ 50% wider when viewed through the glass. The axial magnification effects are small because the external taper of the nozzle (well outside the view of view) is small and the fluid and glass indices nearly match.*

From the whole velocity field, only the average velocity at approximately 80µm above the nozzle opening was extracted from 100 consecutive velocity maps; covering the complete cycle of one single jetting process, see Fig. 3. This central velocity was used in order to be able to neglect the radial correction for the distortion of the image, due to refraction at the air-glass and the glass-fluid interfaces. Axial correction due to the tapering nozzle profile is finite but effectively negligible on the micron scale. Therefore the central velocity analysis can be directly applied to image pixel data, on a linear scale determined by the actual nozzle exit diameter and by the pixel width of the exit as viewed from air (as the width viewed through the glass is magnified by refraction). The velocity response extracted from this point is shown in Fig. 3.
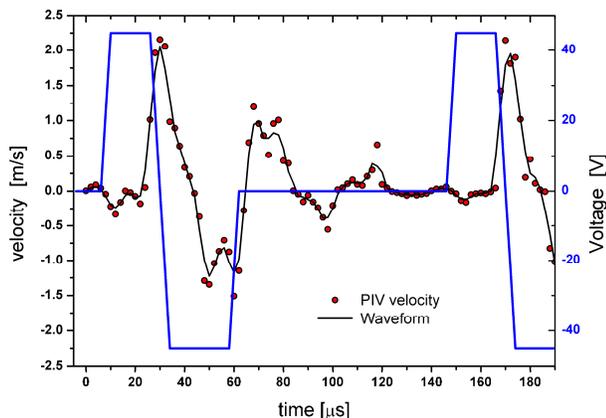

Figure 3. Time variation of the fluid velocity as measured by PIV. See Figure 2.

Numerical method

The simulations were performed using computational methods similar to those reported in [2] [3]. In brief, the numerical simulations used a Lagrangian finite-element method first developed for the study of creeping flow of dilute polymer solutions [5]. The method has since been extended to deal with inertial flows and used to model drop on demand printing of Newtonian and viscoelastic inks [6].

The velocity and pressure fields were discretized over an irregular triangular mesh. An artificial stabilization was employed in order to prevent spurious numerical pressure oscillations [5]. A theta-scheme was used for the discrete time-stepping, and the discrete governing equations were linearized via Picard iteration. Within each iteration, the linear system was solved numerically using the minimal residual (MINRES) method [7]. Adaptive time-stepping was controlled by a CFL condition. The position of each mesh node (except those on the printhead inlet boundary) was updated after each time-step using the converged velocity solution. To maintain element shape quality throughout the simulations, local mesh reconnections were made between time-steps in regions where significant element distortion had occurred. The criteria for reconnection were based on the geometric optimality of the Delaunay triangulation [8]. The local mesh resolution was also maintained by the addition of new nodes in depleted regions, and

the removal of nodes in congested regions. In order to represent the capillary breakup of thin fluid threads, the fluid domain was subdivided artificially when the thread radius fell below a certain threshold (here taken as < 1% of the nozzle outlet radius). A more detailed discussion of the capability of the simulations to capture pinch-off dynamics on a finer scale is given in [2]. No method of coalescence was implemented in the simulations.

A cylindrical coordinate system $\{r,\theta,z\}$ was used to describe the jet, with the origin taken as the centre of the nozzle outlet. The governing equations are the Navier-Stokes equations, which we present below in their dimensionless form (taking the characteristic length scale to be the nozzle outlet radius $d/2$ and the velocity scale to be the target droplet speed v):

$$\partial u/\partial t + (u\cdot\nabla)u = -\nabla p + \nabla^2 u/\text{Re} , \quad \nabla\cdot u = 0,$$

where t, u, and p are the dimensionless time, fluid velocity, and pressure respectively, and Re is the Reynolds number. Gravitational effects are negligible on the length scales considered in this study; the magnitude of the dimensionless gravity term is less than 1.6×10^{-5} for the present experimental parameters. Drag due to air resistance was also neglected in the simulations.

The shape of the printhead used in the simulations was chosen to replicate that of the MicroFab nozzle used in the experiments, while simplifying the interior of the printhead behind the nozzle. The initial finite-element grid is shown (horizontally) in Fig. 4. The top boundary of the grid is the printhead inlet, at which a time-dependent plug flow velocity pulse $V\_P(t)$ was imposed in the axial direction to represent the ink ejection mechanism in the experiments. The bottom boundary of the grid is the nozzle outlet. The initial shape of the fluid meniscus was flat, as in the experiments. The remaining curved boundaries of the grid are the rigid interior walls of the nozzle, at which boundary conditions of no-slip were imposed. Axisymmetry about the z-axis (the jet axis) was assumed throughout. The boundary conditions at the free surface are those of zero shear-stress and the interfacial pressure discontinuity due to the surface curvature

$$\hat{\imath}\cdot\tau\cdot\hat{\jmath}=0, \quad \text{and } [\tau\cdot\hat{\imath}]^{\text{jet}}_{\text{air}}= -1/\text{We}(1/R_1 +1/R_2)\,\hat{\imath},$$

where τ is the stress tensor, $\hat{\imath}$ and $\hat{\jmath}$ are the unit normal and tangent vectors, We is the Weber number and R_1 and R_2 are the principal radii of curvature of the free surface. It was assumed that the external air pressure was a negligible constant. Between time steps the location of the free surface was updated automatically since the finite-element mesh was Lagrangian and mesh nodes (including those on the interface) are advected with the local fluid velocity. The contact line between the interface and the interior walls of the nozzle was held pinned at the edge of the nozzle outlet. The fluid within the printhead was assumed to be initially at rest.
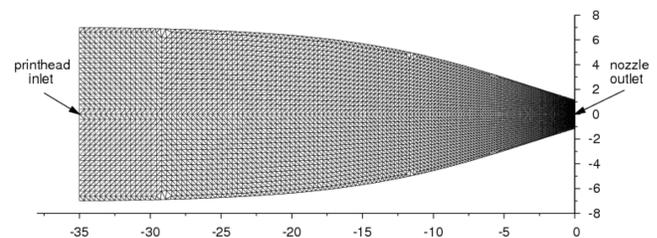

Figure 4. Initial grid used in simulations. Axisymmetry is assumed. The unit of length is the nozzle radius $d/2 = 40$ µm.
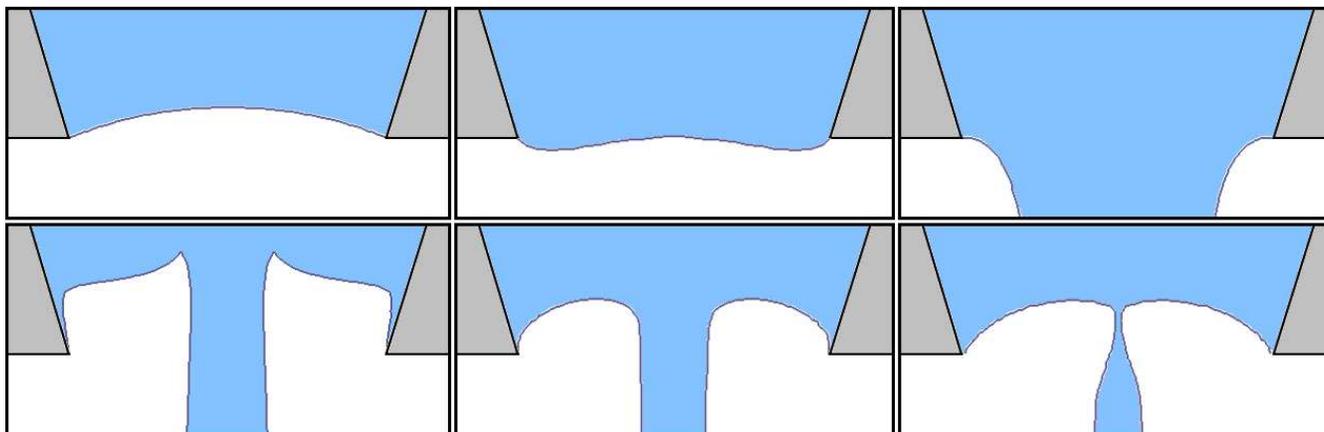
Figure 5. *Fluid boundaries as calculated by Lagrangian simulations, times consistent with those at Figure 2. The unit of length is the nozzle radius d/2 = 40 μm.*

In order to generate droplets in the simulations, a time-dependent axial velocity pulse was prescribed uniformly at the printhead inlet. While this was not expected to accurately model the experimental flow throughout the entire printhead, it was designed to produce sufficiently similar flow conditions in the vicinity of the nozzle cone to yield a reasonable correspondence between simulated and experimental drop shapes and speeds. The shape of the waveform pulse was represented by a simplified piecewise parabolic `push-pull-push' curve [6] or a spline curve fitted to the experimental velocity data obtained by PIV measurements. Reynolds and Weber numbers were matched with those of experimental conditions; Re = 26.8 and We = 43.5 and the amplitude of the waveform was scaled to calibrate the drop speed to ~ 6 m/s.

Some results from the simulations are presented in Fig. 5. Note that in our coordinate system the positive *z* direction is vertically downwards.

Conclusions

Particle image velocimetry studies have been carried out in similar systems in the past [9] but they relay on the flow repeatability to obtain the complete history of the jetting process. In this work, ultra high speed imaging was used to overcome that limitation. Ultra high speed PIV has been successfully demonstrated for 80μm drop on demand jetting within tapered glass nozzles, giving additional input for numerical simulations of inkjet printing performance. The accuracy of the present results is limited by the unknown radial distributions for the velocity and the particles, but lie below the true central velocity within a worst case factor of 2. In addition, experimental results were utilized to set the initial conditions of Lagrangian simulations and results compared with good agreement.

Acknowledgements

References

[1] A.U. Chen and O.A. Basaran, "A new method for significantly reducing drop radius without reducing nozzle radius in drop on demand drop production", Phys. Fluids 14 L1 (2002).

[2] J.R. Castrejon-Pita, N.F. Morrison, O.G. Harlen, G.D. Martin and I.M. Hutchings, "Experimental and Lagrangian simulations on the formation of droplets in drop-on-demand mode", Phys. Rev. E 83, 036306 (2011).

[3] J.R. Castrejon-Pita, N.F. Morrison, O.G. Harlen, G.D. Martin and I.M. Hutchings, "Experimental and Lagrangian simulations on the formation of droplets in continuous mode", Phys. Rev. E 83, 016301 (2011).

[4] R. Adrian, "Particle imaging techniques for experimental fluid dynamics", Ann. Rev. Fluid Mech. 23 261 (1991).

[5] O.G. Harlen, J.M. Rallison and P. Szabo, "A split Lagrangian-Eulerian method for simulating transient viscoelastic flows", J. Non-Newtonian Fluid Mech., 60, 81 (1995).

[6] N.F. Morrison & O.G. Harlen, "Viscoelasticity in Inkjet Printing", Rheologica Acta 49, 619 (2009).

[7] C.Paige and M. Saunders, "Solutions of sparse indefinite systems of linear equations", SIAM J. Numer. Anal., 12, 617 (1975).

[8] H. Edelsbrunner, "Triangulations and meshes in computational geometry", Acta Numerica, **9**, 133 (2000).

[9] C.D. Meinhart and H. Zhan, "The Flow Structure Inside a Microfabricated Inkjet Printhead" Journal of Microelectromechanical Systems 9, 67 (2000).

Author Biography

J.R. Castrejón-Pita received his MSc in Physics (Fluid dynamics) from the National University of Mexico (UNAM, 2003) and his PhD in Physics (Quantum Optics) from the Imperial College (2007). Since then, he has worked in the Inkjet Research Centre at the University of Cambridge. His current research is focused in measurement techniques in DoD and CIJ systems. Rafael is a senior member of Wolfson College Cambridge.

The paper will be presented by Stephen Hoath